IEEE Access
Multidisciplinary | Rapid Review | Open Access Journal

Received April 10, 2022, accepted April 30, 2022, date of publication May 3, 2022, date of current version May 11, 2022.

Digital Object Identifier 10.1109/ACCESS.2022.3172422

Microgrids Operation by Considering Demand Response and Supply Programs in the Presence of IGDT-Based Reverse Risk

MEHRDAD MOVAHEDPOUR[1], MOHAMMAD JAVAD KIANI[1], MAHMOUD ZADEHBAGHERI[1], AND SIRUS MOHAMMADI[2]

[1]Department of Electrical Engineering, Islamic Azad University, Yasuj Branch, Yasuj 7591493686, Iran
[2]Department of Electrical Engineering, Islamic Azad University of Gachsaran, Gachsaran Branch, Gachsaran 7581863876, Iran

Corresponding authors: Mohammad Javad Kiani (kianiph@gmail.com) and Mahmoud Zadehbagheri (mzadehbagheri@gmail.com)

ABSTRACT Concerning the advantages of smart microgrids and the importance of selecting and using technologies accustomed to optimized planning and design of typology and capacity of supplies, demand response programs, and energy-storage charges, existing research has focused on the optimized design of microgrids using ant colony optimization algorithm. Conditions of the optimization problem are enacted on the objective function based on the technical and operational limitations of supplies and microgrids, which may lead to the limitation of response space of the problem. Additionally, a methodology is proposed for modeling and analyzing a novel design to consider the uncertainty of production and demand with reverse risk in the design of residential microgrids. The proposed methodology focuses on the uncertainty of photovoltaic production and load demand by solving two-dimensional multipurpose optimization problem based on information gap decision theory (IGDT). In the mentioned approach, the photovoltaic generation's uncertainty and charge of photovoltaic generation are integrated into an equation to be solved as a problem. Regardless of the likelihood density function of uncertainty parameters and without preparing a firm framework, the current method integrates wind and photovoltaic production into the microgrids. The results of the mentioned method are conclusive, which make the problems solvable.

INDEX TERMS Ant colony algorithm, distributed generation units, demand response, IGDT, microgrid, multipurpose stochastic optimization.

ABBREVIATION

ACO	Ant Colony Optimizatio.
ACSC	Annual Capital Service Cost.
DRP	Demand Response Programming.
DG	Distributed Generation.
DNO	Distribution Network Operato.
DPF	Distributed Particle Filter.
DER	Distributed Energy Resources.
EMS	Energy Management System.
GA	Genetic Algorithm.
GHG	Green House Ga.
IMO	Independent Market Operator.
IGDT	Information Gap Decision Theory.
MO	Market Operator.
MMG	Multi-Microgrids.
MG	Main Grid.
O and M	Operation and Maintenance.
PSO	Particle Swarm Optimization.
PV	Photovoltaic.
RER	Renewable Energy Resources.
ROA	Return On Assets.
RTP	Real Time Pricing.
WT	Wind Turbine.

The associate editor coordinating the review of this manuscript and approving it for publication was Youngjin Kim.

I. INTRODUCTION

Because the various equipment installed in microgrids, and the different types of technology, capacity, technical parameters, investment expenses, and productivity, there is a wide range of responses to microgrid design problems. So, to determine the optimized response, the design problem of microgrids can be stated as an optimization problem aimed at

minimizing of expenses of the microgrid design. Recently, attemots have been made to design an optimized microgrid model. Nevertheless, a few studies have focused on optimized modeling of residential microgrids. The optimized design of microgrids has been investigated as a case study. Robust optimization has been used for local distributed generation units to minimize investment, productivity, and pollution expenses [1]. Capacity planning is investigated separately [2]. Determination of optimized energy storage capacity in microgrids to minimize expenses is investigated [3]. The environmental effects of installing wind and photovoltaic units and diesel units in remote microgrids are investigated [4], [5]. An optimal microgrid design was established considering load and PV power output uncertainties to promote the supply-demand balance using the particle swarm optimization (PSO) algorithm [6]. Some other papers have studied the multi-objective problem in multi-grid networks. Ref [7] designed a market operator (MO) and a distribution network operator (DNO) for a network of microgrids in consideration of multiple objectives. In [8], a new market mechanism has proposed to quantify the value of emergency energy transactions in renewable-based multi-microgrid (MMG) systems. Ref [9] addressed the energy dispatch problem for multi-stakeholder multiple microgrids (MMGs) under uncertainty while considering independent market operators (IMOs). Ref [10] has done an optimal design of microgrid considering the dynamic state of distribution units by distributed particle filter (DPF) technique. The development design of microgrids, including distributed generation units and CHP, is investigated to minimize investment, productivity, and pollution expenses in microgrids [11]. A novel method is proposed for the design and productivity of microgrids connected to the network. The mentioned method is based on a decision tree [12]. In the research, as mentioned earlier, the design of microgrids is generally discussed, and there has not been a point related to residential microgrids. The optimized capacity of photovoltaic units and batteries installed in residential microgrids is calculated to minimize annual expenses [13]. A residential microgrid model including wind-power and photovoltaic units is discussed. The design problem of residential microgrids is expressed as an optimization problem in this research which is investigated using PSCAD in order to evaluate the effect of these units and other parameters on the microgrid [14]. In other researches which have focused on the same subject, potential effect of EVs and inflexible charges are investigated [15]–[19]. Short-term planning of smart grids has been done to find the optimized control on economic distribution in DSM [20]–[27]. Due to the usage of renewable resources in microgrids, some of the parameters, including spatial factors, temperature, sunray, and wind speed, can affect the output of photovoltaic systems. These parameters can lead to unexpected changes in PV output [28], [29]. Under the mentioned conditions, suitable methods and approaches must be used to compensate for the complications arising due to the uncertainty of wind and photovoltaic power plants, which affect the productivity of microgrids. For instance, modeling the uncertainty of renewable resources using random techniques and fuzzy approaches has been investigated in many studies [15], [18]. Although advantages of the mentioned techniques have been discussed, these techniques are not free of disadvantages. For instance, random methods such as Monte Carlo [17], [19], scenario-based modeling [16], [30], and point estimation [20] cannot predict uncertainty without probability density function. The fuzzy technique needs a membership function. Additionally, fuzzy numbers are not easy to work with [21]. Recently, information gap decision theory (IGDT) has been a promising method for applicable industrial programs in order to deal with uncertainty. Specially, power system engineers who try to reduce productivity expenses are into using the mentioned method, IGDT. Accordingly, this theory is no dependent upon information related to past inclination of uncertainty parameters [22], [23]. For instance, options of purchasing energy for retailers and wholesalers are mentioned by [24] and [25] respectively. Optimized production strategies of power markets are mentioned based on IGDT [26]. Additionally, [27] have met demands arisen for huge electric consumption based on IGDT. The known theory of IGDT explains uncertainty of power production in wind plants [23], [31]–[34]. However, daily changes of uncertainty parameters are not investigated. Ref [35] focus on IGDT for models based on UC concerning the uncertainty of wind plants and regardless of simultaneous uncertainty. A hierarchical management system of frequency and energy is mentioned, composed of an island microgrid [36]. However, values of uncertainty parameters are not investigated simultaneously. The novelty of this work lies in the creation of an integrated latent model that takes advantage of different aspects and features of energy consumption in modern energy systems. One of the designed microgrid features is that the load flexibility obtained by using demand response smart grid programs that plan high-consuming electrical appliances like washing machines, dryers, dishwashers, and electric cars is intended to user benefit rather than user benefit their random access. In this paper, in order to evaluate the efficiency of the designed microgrid from the economic and reliability perspective, error occurrence and blackout likelihood in residential microgrids are also considered. Due to error in the connection line between the microgrid and the main grid or in the generation units in the microgrid, in some hours the microgrid may not be able to provide part of the consumption load. This leads to subscribers' power outage and blackout which has been considered in the optimal design of the residential microgrid. More importantly, in order to increase the strength and resistance of the designed system, a risk-averse strategy has been used in the face of uncertainty parameters. In this strategy, the uncertainty of the parameters will have a negative impact on the objective function, so that the actual power of the consumption load is greater than the predicted power, and the actual generation power of the renewable units is considered less than their predicted power. The maximum radius of uncertainty in the generation of renewable wind, photovoltaic, and load resources

will be achieved by implementing the IGDT method via solving a multi-objective optimization problem, to determine the strength and resilience of the designed microgrid against uncertainty parameters for decision makers. The proposed method considers the uncertainty of photovoltaic and wind power generation and load demand simultaneously with solving the problem of optimizing two-level multi-objective using IGDT theory. At the first level, it is assumed that the predicted value for generating renewable resources and system load demand is equal to their actual values. At this level, the objective function of the problem is the annual cost of the microgrid. After optimizing the problem at the first level and determining the minimum annual cost of the microgrid by considering a critical cost for the objective function to deal with uncertainties, in the second level the maximum radius of uncertainty of wind and photovoltaic units, and consumption load is calculated using IGDT theory so that the microgrid resistance to these uncertainties can be measured. Another feature of this article compared to previous researches is the use of the ant colony optimization algorithm for the stochastic design of residential microgrids due to the existence of discrete variables in problem modeling. Therefore, the operations mentioned above are matched with principles of a smart grid this model can be used for large-scale modeling including operational patterning with no need of burdening calculations.

II. FORMULATION

The recommended method is enacted on a residential microgrid in Okinawa, Japan [37]. The block diagram is shown in Figure 1. Thus, to determine the strength and resistance of the system for supplying the required demand, the maximum uncertainty radius of wind and photovoltaic resources and consumption load are taken into account based on IGDT by solving a multipurpose optimization problem. Time considered in a model is $\Delta t = 1$ which is discarded to simplify the equations.

A. POWER BALANCE

According to Figure (1), injection power of wind and photovoltaic units and diesel and main networks includes two currents of AC and DC. According to the following equations, power balance can be kept stable for buses of AC and DC separately.

$$p^{ac}_{wt}(t)+h_{DC/AC}\left[p^{ac}_{pv}(t)+p_{Dch}(t)\right]+p^{ac}_{PG}(t)=p_L(t)+p_{SG}(t) \quad (1)$$

$$\eta_{AC/DC}\left[p^{dc}_{WT}(t)+p^{dc}_{PG}(t)\right]+p^{dc}_{PG}(t)=p_{ch}(t) \quad (2)$$

According to the fact that production of renewable resources fluctuates and can be affected easily, renewable production can be way higher than consumption. Therefore, renewable production can be limited based on the following restrictions which can restrict power distribution:

$$p^{ac}_{WT}(t)+p^{dc}_{WT}(t) \le N_{WT}.p_{WT_1}(t) \quad (3)$$

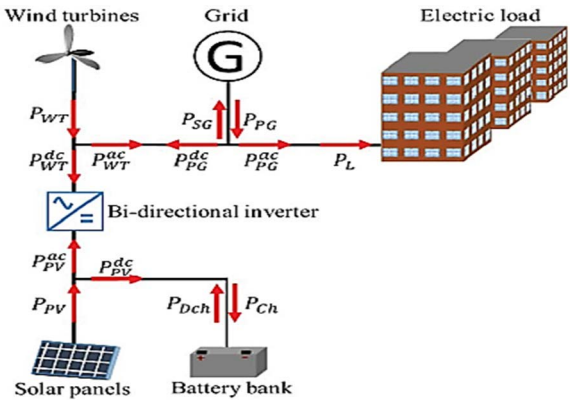

FIGURE 1. Block diagram of the proposed microgrid.

$$p^{ac}_{PV}(t)+p^{dc}_{PV}(T) \le N_{PV}.p_{PV1}(t) \quad (4)$$

The power which is sold to or purchased from the main grid cannot exceed the maximum amount mentioned in the contract:

$$p^{ac}_{PG}(t)+p^{dc}_{PG}(t) \le u(t).\underline{p_G} \quad (5)$$

$$p_{SG}(t) \le (1-u(t).\underline{p_G} \quad (6)$$

Generally, u is the only binary variable. This variable restricts purchasing power from and selling power to the main grid, which is impossible in the real world. According to the following equation, the production capacity of 1 kWh of wind unit per hour can be explained as a function of wind speed and parameters of wind turbines:

$$p_{WT1}(t)=\begin{cases} 0, & if\ v(t)<v_{ci}\ or\ v(t)>v_{ci}\ or\ v(t)>v_{co}\dfrac{v^3(t)-v^3_{ci}}{v^3_r-v^3_{ci}} \\ & if\ v(t)>v_{ci} \\ & and\ v(t)<v_r 1, \quad if\ v(t)>v_r\ or\ v(t)<v_{co} \end{cases} \quad (7)$$

Value of the parameters v_{ci}, v_r and v_{co} are 3, 10, and 20 m/s, respectively. The diagram is shown in Figure 2 [37].

According to [37], N_{WT} is considered a continuous variable. Production output of 1 kWh for a photovoltaic unit can be stated as a function of I_G and T_a:

$$T_c(t)=T_a(t)+I_G(t)\frac{NOCT-20}{0.8} \quad (8)$$

$$p_{PV1}(t)=Y_d\frac{I_G(t)}{I_s}\left[1-\frac{K_p}{100}(T_c(t)-T_{STC}\right] \quad (9)$$

In the above equation, IG per hour depends on the solar panel's inclination angle, 30 degrees as the optimized angle [37].

B. CHARGE AND DISCHARGE MODEL OF THE BATTERY

The balance of energy equation for a batter is explained as follows:

$$Q_B(t+1)=Q_B(t)+\eta_r p_{ch}(t)-p_{Dch}(t) \quad (10)$$

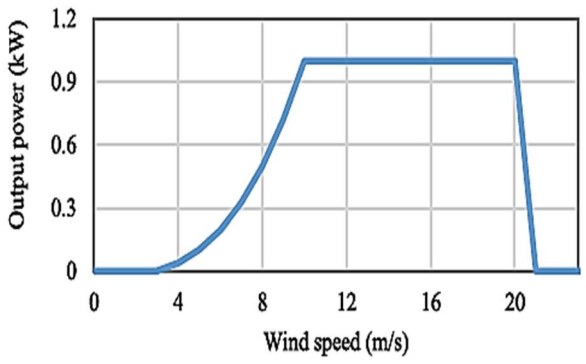

FIGURE 2. The output curve of a 1kw wind turbine.

In the equation mentioned above, energy stored in the battery at $t+1$ is a function of energy stored at t and the amount of charge and discharge at t. According to the following equations, energy stored in the battery per hour is limited by the minimum and maximum value of SOC:

$$Q_B(t) \leq SOC.N_B - Q_f(t) \tag{11}$$
$$Q_B(t) \geq SOC.N_B \tag{12}$$

The total reduction of battery capacity at every time can be calculated as the following:

$$Q_f(t+1) = Q_f(t) + Z_B.p_{Dch}(t) \tag{13}$$

According to the above equation, ZB expresses the linear depreciation coefficient, which is investigated in some research for all battery technologies based on long-term measurement of the electric field in the energy storage system. To make sure that all energy expenses are taken into account, energy stored in the battery at the end of the period must be more than the energy at the beginning:

$$Q_B(|T|) \geq SOC_0.N_B \tag{14}$$

According to the following equations, the charge and discharge battery's power is restricted by technical features of the battery:

$$P_{ch}(t) \leq N_B.\underline{p_B} \tag{15}$$
$$p_{Dch}(t) \leq N_B.\underline{p_B} \tag{16}$$

C. INVERTER MODEL

According to the following equation, the nominal capacity of the bilateral inverter must be bigger than electrical power passing through the inverter in both directions of AC to DC and vice versa:

$$\eta_{DC/AC}\left[p_{Dch}(t) + p^{ac}_{PV}(t)\right] \leq N_{Inv} \tag{17}$$
$$\eta_{AC/DC}\left[p^{dc}_{WT}(t) + p^{dc}_{PG}(t)\right] \leq N_{Inv} \tag{18}$$

D. CONSUMPTION LOAD MODEL

In the current paper, consumption load is explained in three ways: Thermal load: TRNSYS software packages are used to predict the annual thermal load required for a Japanese household living in a 100 m^2 one-story building in Okinawa. According to Figure 3, the consumption load of residential microgrids can be calculated by multiplying the figure's height by the number of houses.

Uncontrollable appliances: Every house is laden with uncontrollable appliances such as cooking machines, hairdryers, vacuum cleaners, lighting, and computers. PNCL indicates these devices.

1) CONTROLLABLE LOADS

In Table (1), three different patterns of charging time of automobiles are mentioned.

According to this modeling methodology, to reduce the problem dimensions and the time required for optimizing consumption loads, both uncontrollable and controllable consumers must be included in the problem. Total consumption load is bigger than or equal to uncontrollable and controllable consumption loads plus unsupplied energy. This equation can be true for every interval at T:

$$\sum_{t\in H_i} p_L(t) \geq \sum_{m\in A} N^m_{App} p^m_{App} D^m_{App} F_{i,m} + \sum_{t\in H_i} p_{NCL}(t) \tag{19}$$

In the above relation, $F_{i,m}$ indicates the minimum operational time for m during H_i to D^m_{App} ration, which is shown as the following:

$$F_{i,m} = 1 - \min\left\{\frac{k_{i,m}}{D^m_{App}}, 1\right\} \tag{20}$$

Some appliances such as washing machines must be kept on continuously when they are supposed to be used. Some other appliances, such as electric cars, do not need to be continuously connected to the network. They can be charged for an hour, and then they can be disconnected. It is possible to charge them later again. In this relation, $K_{i,m}$ indicates maximum continuous hours H_i/H_m; required for each appliance (m). Additionally, this parameter shows the total hours H_i/H_m; an appliance is on continuously (such as charging electric cars). According to the following relation, consumption load at $t \in T$ must be bigger than or equal to uncontrollable subtraction loads from unsupplied loads at the same time to make sure that controllable loads are supplied:

$$p_L(t) \geq p_{NCL}(T) \tag{21}$$

The following relation shows that for every D-hour period, the total consumption load is equal to the sum of controllable and uncontrollable loads at the same period:

$$\sum_{t=1}^{D} p_L(t) = \sum_{m\in A} N^m_{App} p^m_{App} D^m_{App} + \sum_{t=1}^{D} p_{NCL}(t) \tag{22}$$

Some appliances need a network connection for more than an hour to work. According to table 1, an electric car needs

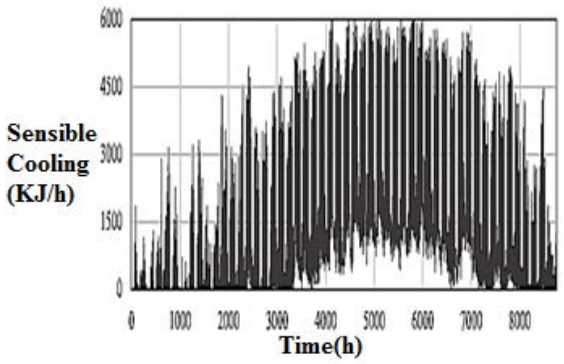

FIGURE 3. The profile of annual consumption load for a 100 m^2 residence in Okinawa, Japan [37].

TABLE 1. The electrical appliances and their features.

Appliance	Power (kW)	Duration (h)	Usage Freq	Shifting Window
Washing machine	o.5	1	0.7	(07:00-24:00)
Cloth dryer	1	1	0.7	(07:00-24:00)
Dishwasher	0.9	1	1	(18:00-24:00)
EV1	2	3	0.4	(00:00-07:00)
EV2	2	3	0.3	(18:00-24:00)
EV3	2	3	0.3	(00:00-24:00)

3 × 2kWh, which means 2 kWh for 3 hours. Therefore, to prevent responses that may lead to energy accumulation in an hour, for example, 1 × 6kWh for electric cars, the following relation is used to find the most suitable solution for the problem:

$$p_L(t) \le \sum_{m \in A} N^m_{App} p^m_{App} Z_{t,m} + p_{NCL}(T) \tag{23}$$

Binary coefficient $Z_{t,m}$ is calculated based on consumption time:

$$z_{t,m} = \begin{cases} 1 & if\ t \in \mathrm{H}_m \\ 0 & if\ t \notin \mathrm{H}_m \end{cases} \tag{24}$$

E. OBJECTIVE FUNCTION

The objective function of the mentioned problem minimizes the annual grid expenses (ACS). Annual grid expenses include purchase, operation, maintenance (O&M), replacement and purchasing power from the main grid, and outage expenses (unsupplied energy). It is worth noting that profit made out of selling power to the grid is taken into account negatively. Accordingly, the objective function for the residential microgrids is defined as:

$$ACS = P2A \times \begin{bmatrix} N_{pv}(pv_{Aq} + pv_{OM} \\ + N_{Inv}(Inv_{Aq} + Inv_{OM} + Inv_{Rep}) \\ + N_B(B_{Aq} + B_{OM}) + Q_f(|T|)B_{Rep} \end{bmatrix}$$

$$+ N_{day} \sum_{t \in T} \left[C_p(t)(p^{ac}_{PG}(t) + p^{dc}_{PG}(t)) - C_s(t) p_{SG}(t) \right] \tag{25}$$

The period is taken three years. In relation (25), $Q_f\ (|T|)\ B_{Rep}$; indicates the loss of battery value reduction due to reduced capacity, and it is expressed as the multiplication of battery capacity at the end of the optimization period by replacement expenses. Photovoltaic and wind units do not need replacement expenses to be considered, while inverters need one replacement. All expenses must be calculated annually (annual value). In (25), all expenses must be mentioned annually to express objective function as the function of annual expenses of the considered grid. Because the microgrid simulation is performed only for one day (T), the amount of power bought from the main grid and sold to the same grid plus unsupplied energy expenses are related to the same day. Therefore, to express the expenses annually, the number of days must be taken into account to calculate the annual operating expenses of the microgrid. Purchase, operation and maintenance expenses, and replacement costs (Table 4) can be indicated in present value. According to [33], the present value coefficient is multiplied by P2A (250). The present value coefficient is calculated as the following:

$$p2A = \frac{I_{\text{int}}(1 + I_{\text{int}})^{EL}}{(1 + I_{\text{int}})^{EL} - 1} \tag{26}$$

Variables of optimized design for microgrids problem are:

Variable 1: installed capacity of wind turbine (N_WT)

Variable 2: installed capacity of photovoltaic panels (N_PV)

Variable 3: installed capacity of the battery (N_B)

Variable 4: installed capacity of the inverter (N_Inv)

Variables 5-16: operation hours of appliances as controllable loads, which are expressed as the following:

Variable 5: operation hours of appliance 1 (washing machine)

Variable 6: operation hours of appliance 2 (clean-dryer machine)

Variable 7: operation hours of appliance 3 (dishwasher)

Variables 8-10: operation hours of appliance 4 (EV1 car) which is 3 hours

Variables 11-13: operation hours of appliance 5 (EV2 car) which is 3 hours

Variables 14-16: operation hours of appliance 6 (EV3 car) which is 3 hours.

Accordingly, variables of the optimization problem can be expressed as $X = [x_1, x_2, \ldots, x_i, \ldots, x_{n-1}, x_n]$; in which has gotten 16 members. Variables 5-16 are related to the operation time of controllable appliances. Operation time is calculated by the ACO optimization algorithm, which is generally used to control when response loads are connected to the microgrid.

ACO flowchart is shown in Figure 4.

Stage 1: Information related to input data and system (Tables 4 and 5) as well as parameter regulation of ACO

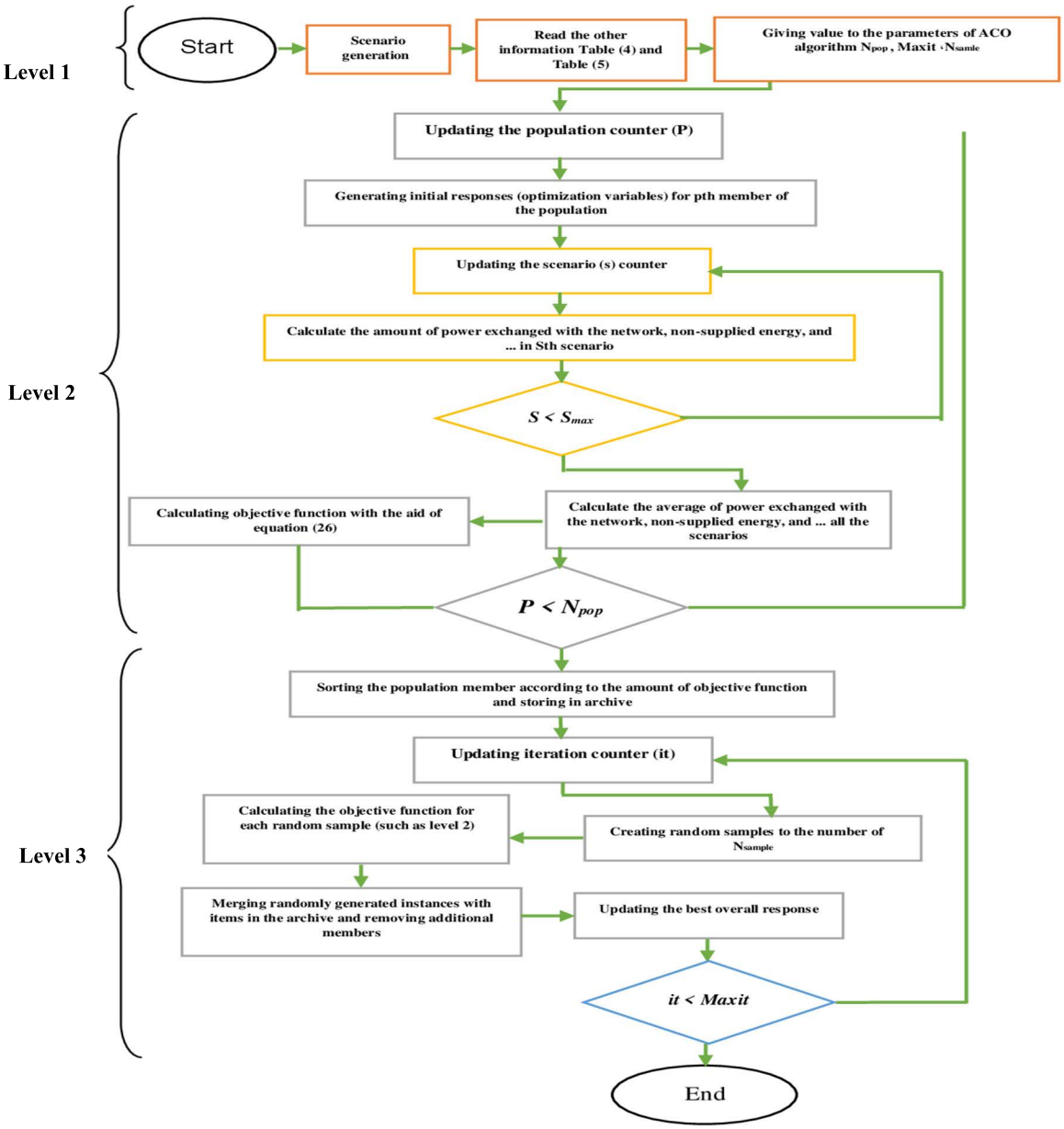

FIGURE 4. The flowchart of the ACO algorithm.

algorithm is investigated. Weighted coefficient and likelihood in the ACO algorithm are calculated for variables of the optimization problem.

Stage 2: This step focuses on producing primary responses, including optimization variables for each member of the population. For each member of the population, which is a 16-member vector of optimization variables, the purchasing power (AC and DC) or the power sold to the main grid (AC), reduction of battery capacity, and supplied power are calculated. Finally, the objective function of each member is determined based on (25).

Stage 3: After generating primary responses and objective functions for each member, the responses and objective functions are put in order and saved in the archive. Random samples are produced based on the probability model for the N_{sample}. The value of the objective function is calculated for each random sample. Random samples are merged with archived ones to delete outliers. The mentioned process repeats until the repetition number of the algorithm finishes.

III. INFORMATION GAP-BASED DECISION THEORY

IGDT method can compensate uncertainty of information-deficit problems to make the optimized decision [22]. The strength function expresses the most considerable uncertainty (failure is impossible) [31], [38]. Assume that the indefinite input parameters vector is indicated by R. Then, X can be a

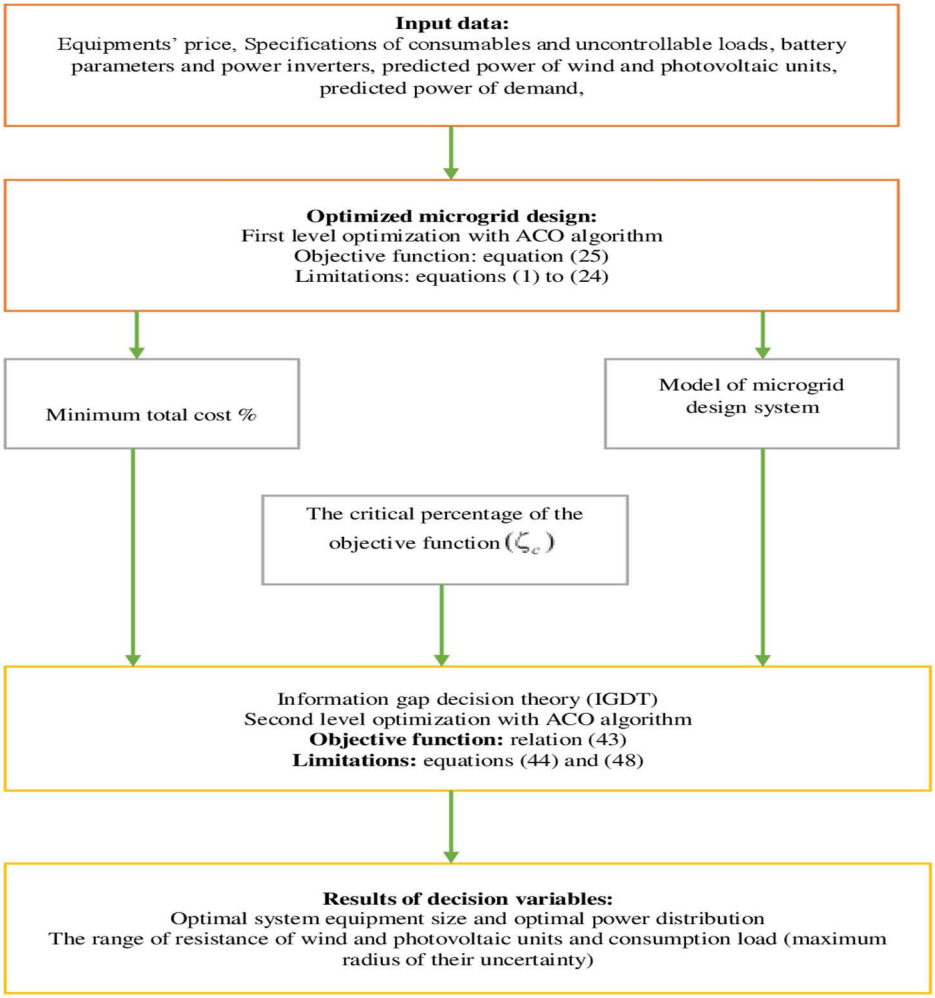

FIGURE 5. The flowchart of the proposed method (two-level optimization).

set of decision variables, and Γ can show a set of uncertainty. Unknown input parameters behave like the following:

$$\forall \gamma \in \Gamma\left(\underline{\gamma}, \zeta\right) = \left\{\gamma : \left|\frac{\gamma - \underline{\gamma}}{\underline{\gamma}}\right| \leq \zeta\right\} \tag{27}$$

In the above mentioned, γ shows the uncertainty parameter and $\underline{\gamma}$ is the predicted value of the uncertainty parameter. ξ indicates the maximum deviation of the uncertainty parameter from the predicted value. This coefficient is called uncertainty radius. Accordingly, the strength function is:

$$\hat{\zeta}\left(X, R_C\right) = \left\{\zeta : R\left(X, \gamma\right) \geq R_C \; \gamma \in \Gamma\left(\underline{\gamma}, \zeta\right)\right\} \tag{28}$$

In the above relation, $R\left(X, \gamma\right)$; symbolizes the system model. The least requirement of the system can be set by RC. Strength function is shown by $\hat{\zeta}\left(X, R_C\right)$. It is worth noting that strength value is dependent on decision variables and the least requirements asked by RC. According to the mentioned relation, the general optimization problem is:

$$f(x, \gamma) \tag{29}$$

$$(x, \gamma) \leq 0, \quad i \in \Omega_{ineq} \tag{30}$$

$$\gamma \in \Gamma \tag{31}$$

It is stated that there are no differences between uncertainty and predicted parameters:

$$f_0 = f(x, \gamma) \tag{32}$$

$$(x, \gamma) \leq 0, \quad i \in \Omega_{ineq} \tag{33}$$

$$(x, \gamma) = 0, \quad j \in \Omega_{eq} \tag{34}$$

The initial value of the objective function shown by fo can be calculated via (34) - (36). If the uncertainty parameter exceeds the predicted value, decision-makers face two different risk-taking and risk aversion strategies. The risk aversion strategy is used for information analysis in the current study. To this end, the uncertainty parameter negatively affects the objective function. Uncertainty parameters can lead to an increase in the objective function. Therefore, finding the maximum radius of uncertainty parameters for inputs is possible using the mentioned strategy. Conservative decision-makers usually choose this strategy. It is expected

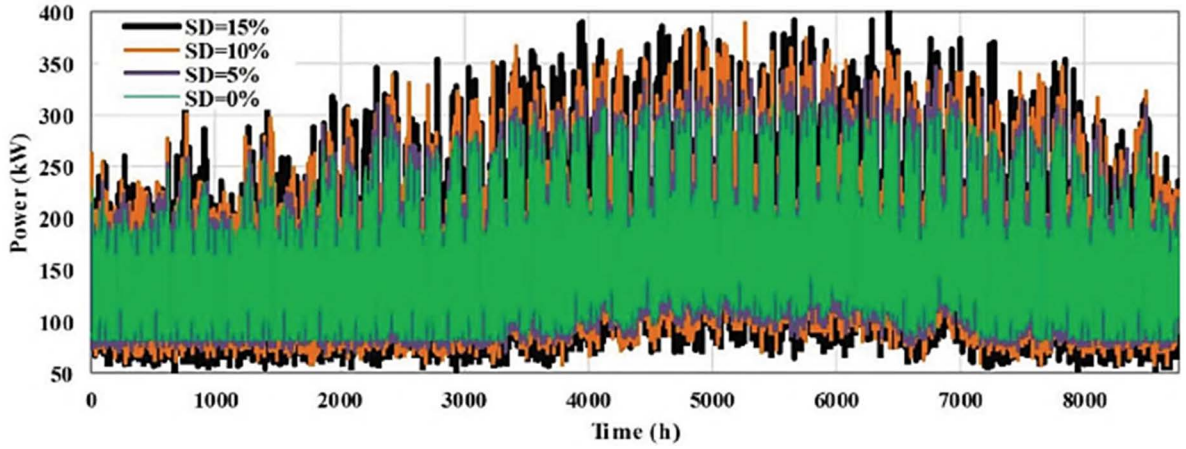

FIGURE 6. The profile of annual uncontrollable load for every deviation of wind standard.

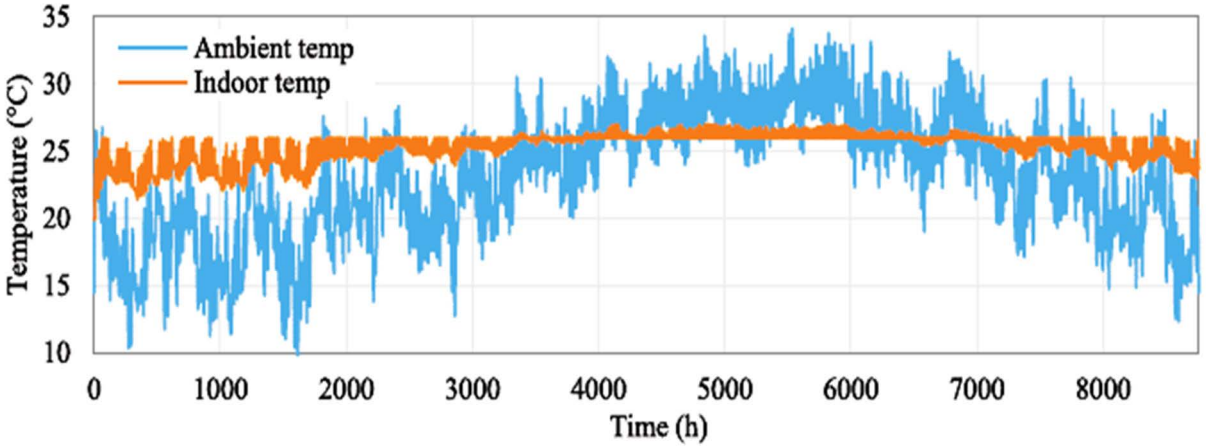

FIGURE 7. The temperature during the year.

to take an optimized set of decision-making variables into account to prevent the objective function from deviation. Also, the uncertainty parameter is quite different from the predicted value. It is worth noting that the maximum strength and resistance can be obtained if the objective function is not affected by the maximum radius of the uncertainty parameter. The mathematics of the strategy can be as the following:

$$\zeta = \zeta \tag{35}$$

$$(x, \gamma) \leq 0, \quad i \in \Omega_{ineq} \tag{36}$$

$$(x, \gamma) = 0, \quad j \in \Omega_{eq} \tag{37}$$

$$\left\{ \frac{f(x, \gamma) \leq \Lambda_c}{\Lambda_c = f_o(x, \gamma) + \varsigma_c \left| f_o(x, \gamma) \right|, \gamma \in \Gamma} \right\} \tag{38}$$

Λ_c shows the critical value that the objective function cannot exceed. Although this parameter can be defined based on decision making requirements, it is defined as a sub-function of f0. Also, ς_c is a positive parameter that is set by decision-makers to be used to define the critical value of Λ_c. Therefore, the mentioned strategy, which is defined for the EMS model, can be expressed as the following:

$$\begin{aligned} J_O = P2A & \\ \times & \begin{bmatrix} (N_{PV}(PV_{Aq} + PV_{OM}) + N_{WT}(WT_{Aq} + WT_{OM}) \\ + N_{Inv}(Inv_{Aq} + Inv_{OM} + Inv_{Rep}) \\ + N_B(B_{Aq} + B_{OM}) + Q_f(|T|)B_{Rep} \end{bmatrix} \\ & + Nday \sum_{t \in T} \left[C_p(t)(p^{ac}_{PG}(t) + p^{dc}_{PG}(t)) - C_s(t)P_{SG}(t) \right] \end{aligned} \tag{39}$$

J_0 indicates the total expenses of the microgrid design (25). On the other hand, it is assumed that the output power of wind and photovoltaic units and power demands are not matched with the predicted values. According to reverse risk, power generation of wind and photovoltaic units is less than the predicted values, while system demand is more than the predicted demands. Accordingly, the following relations are added to the existing ones:

$$\left\{ \xi : \xi = \omega_{wt}\xi^{wt} + \omega_{pv}\xi + \omega_{\iota}\xi^{\iota} \right\} \tag{40}$$

$$J \leq J_o + |J_o| \, \varsigma_c \tag{41}$$

TABLE 2. Data used for simulation.

Average sunlight (kWh/m2)	Average wind speed (m/s)	Average temperature (°C)	Average uncontrollable load (kW)	Total uncontrollable load (kW)	Hour
0.00	7.2220	22.95	0.4407	117.23	1
0.00	6.9345	22.71	0.3726	99.12	2
0.00	6.4055	22.73	0.3404	90.54	3
0.00	5.8880	22.58	0.3296	87.68	4
0.00	5.7845	22.59	0.3870	102.93	5
0.00	5.5775	22.67	0.4479	119.13	6
0.00	4.8530	22.76	0.4694	124.85	7
2.65	4.4160	22.70	0.5052	134.38	8
6.64	4.6805	22.76	0.5948	158.21	9
7.25	4.7265	22.81	0.7381	196.33	10
12.16	4.7265	22.77	0.7596	202.05	11
15.21	4.6575	22.82	0.7847	208.72	12
16.36	4.6575	22.86	0.8277	220.16	13
15.35	4.4505	22.87	0.7882	209.67	14
11.08	4.3125	22.91	0.8062	214.44	15
7.96	4.5540	23.06	0.8241	219.20	16
3.12	4.1630	23.11	0.8348	222.06	17
1.58	3.6800	23.13	0.8527	226.83	18
0.00	4.0365	22.99	0.9316	247.80	19
0.00	4.8875	22.90	0.8062	214.44	20
0.00	5.1405	22.74	0.6127	162.97	21
0.00	5.5545	22.86	0.5625	149.63	22
0.00	6.5320	22.92	0.5410	143.91	23
0.00	7.1415	22.85	0.4801	127.71	24

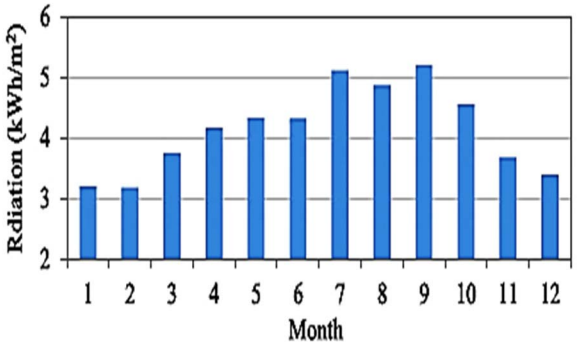

FIGURE 8. The sunlight diagram for 30 ° for every month of the year.

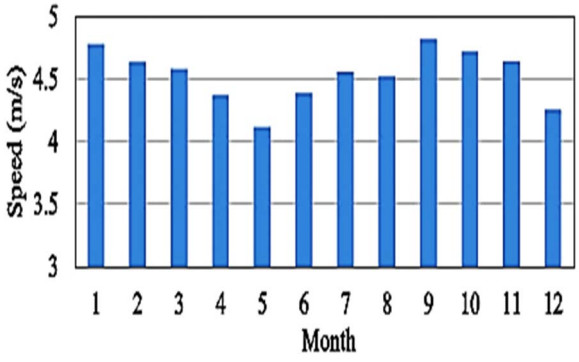

FIGURE 9. The wind speed diagram for every month of the year.

$$P_{PV}^{act} = P_{WT}(1 - \xi^{wt}), \quad \forall t \in T \tag{42}$$
$$P_{PV}^{act} = P_{PV}(1 - \xi^{pv}), \quad \forall t \in T \tag{43}$$

In the above relations, ω_{pv} and ω_{pd} indicate weighted factors for objective functions ξ^{pv} and ξ^{pd}, respectively. It is worth stating that different methods solve multipurpose optimization problems. Among the available methods, we can point to weighted sum, fussy method, and ϵ-limitation methods [39]. According to the fact that the weighted sum is simplified [40], it is used in this study to calculate demand and supply simultaneously. It is worth noting that results obtained from weighted sum can be generalized due to conditions used in the mentioned method. Accordingly, other multipurpose optimization methods can provide the same solutions [41]. P_{WT}, P_{PV} and P_{L} can be replaced by $\text{P}_{\text{WT}}^{\text{act}}$, $\text{P}_{\text{PV}}^{\text{act}}$ and $\text{P}_{\text{L}}^{\text{act}}$ in (1)-(4), (17)-(19), and (21)-(23) to increase the generation of wind and photovoltaic units and reduce loads.

IV. RISK AVERSION OF IGDT BASED ON MICROGRID DESIGN

The following steps should be mentioned to examine the proposed model:

Step 1: preparing classified input information as known and predicted data. Available information includes equipment

TABLE 3. The total uncontrollable load of microgrid for different percentages of demand responses.

Demand response 45% (kW)	Demand response 30% (kW)	Demand response 15% (kW)	Demand response 0% (kW)	Hour
72.96	82.26	102.03	117.23	1
61.69	69.55	86.27	99.12	2
56.35	63.53	78.80	90.54	3
54.57	61.53	76.31	87.68	4
64.06	72.23	89.58	102.93	5
74.15	83.59	103.68	119.13	6
77.70	87.61	108.66	124.85	7
83.64	94.29	116.96	134.38	8
98.46	111.01	137.69	158.21	9
122.19	137.76	170.87	196.33	10
125.75	141.78	175.85	202.05	11
129.90	146.46	181.65	208.72	12
137.02	154.48	191.61	220.16	13
130.50	147.13	182.48	209.67	14
133.46	150.47	186.63	214.44	15
136.43	153.81	190.78	219.20	16
138.21	155.82	193.27	222.06	17
141.17	159.16	197.41	226.83	18
154.22	173.88	215.66	247.80	19
133.46	150.47	186.63	214.44	20
101.43	114.36	141.84	162.97	21
93.13	104.99	130.23	149.63	22
89.57	100.98	125.25	143.91	23
79.48	89.61	111.15	127.71	24

price, equipment features, uncontrollable loads, battery parameters, and inverter parameters. Predicted data for the daily generation of wind and photovoltaic units can be counted as input.

Step 2: according to the inputs prepared in the previous step and formulation of microgrid design, the ACO algorithm named optimization motor triggers problem solving and determination of the optimized equipment sizes and the optimized distribution according to technical requirements mentioned in the previous sections. Then, optimized total expenses can be sent to the following step. It is worth noting that some of the restrictions enacted on the microgrid design are used in the following steps. These restrictions can be taken as the output. This step's number of optimization variables is 16 decision-making variables defined in section 2.

Step 3: the worsening extent of the objective function is selected to determine the exact threshold for total expenses in the face of uncertainty of renewable generation. Decision-makers set the threshold.

Step 4: IGDT can maximize the uncertainty radius of wind and photovoltaic generation based on the ACO algorithm. At the same time, load demand is met based on different restrictions mentioned in step 2 and enacted in step 3 to satisfy the system. The number of optimization variables of this step is 16 decision-making variables mentioned in step 1, 3 decision-making variables mentioned for uncertainty radius of wind and photovoltaic units and consumption load. The maximum value of these three variables is set to maximize objective function in 43 to prevent design expenses from exceeding critical value. The operational results determine the specific interval of demand and supply.

Additionally, precise decision-making about equipment and its distribution is done. The Flowchart mentioned for the following steps can be seen in Figure 5. It is worth noting that the microgrid model can be explained as the summation of the relations mentioned in 48:

V. SIMULATION RESULTS

A simulation of the proposed method has been done for a residential microgrid in Okinawa, Japan [37], as shown in Figure 1. Ant colony optimization (ACO) in MATLAB has been used to simulate the method. The total consumption load for this microgrid is 4000 kWh for 24 hours. The number of subscribers connected to the microgrid is 266. Accordingly, the consumption load of every subscriber is 15 kWh in 24 hours. The effect of controllable loads can be expressed as a percentage of uncontrollable loads. Therefore, demand response is evaluated in 4 steps in which the percentage of controllable demand to consumption load ratio are 0%, 15%, 30%, and 45%, respectively. The diagram of

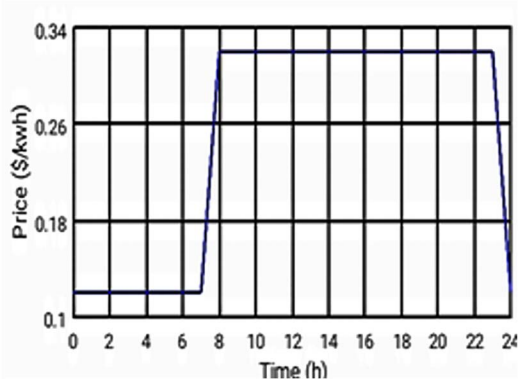

FIGURE 10. New price for purchasing power from the main grid.

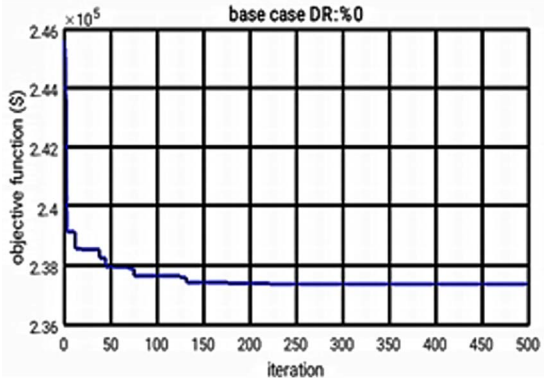

FIGURE 11. The convergence process of the objective function regarding the base for demand response of 0%.

TABLE 4. Economics data for system components.

Initial acquisition costs				Initial replacement costs		Yearly O&M costs
PV ($/kW)	WT ($/kW)	Battery ($/kWh)	Inverter ($/kW)	Battery ($/kWh)	Inverter ($/kW)	2% of initial acquisition costs
3000	2500	195	500	195	500	

TABLE 5. Technical data and fixed values.

Nominal interest rate (%)	Inflation rate (%)	Project lifetime (years)	P_B (kW)	$\underline{SOC}$	$\overline{SOC}$	SOC_0
3.75	1.5	25	0.5	0.2	0.95	0.5
Z_B	$\eta_{DC/AC}$, $\eta_{AC/DC}$	η_r	Y_d	K_p (%/°C)	T_{STC} (°C)	NOCT (°C)
3.10^{-4}	0.93	0.86	1[33]	0.043	25	45.5

the uncontrollable load is shown in Figure 6 for different deviation levels of wind standards. The average amount of uncontrollable load in every hour of the day can be calculated by averaging the annual values. The average temperature for every annual time can be seen in Figure 7. The average temperature for every day can be calculated by averaging the annual values.

The sunlight diagram can be seen in Figure 8.

The wind speed diagram is shown in Figure 9. The average wind speed is 4.68 m/s.

According to the fact that simulation of the microgrid is done for one sample day, weather data and consumption load collected for one year can be averaged for one day to simulate data for one 24-hour day. Table 2 gives the information about averaged uncontrollable consumption load, averaged controllable consumption load for every subscriber, average temperature, wind speed, and sunlight for a 24-hour day. Information related to controllable loads is given in Table 1. To conduct the simulation, it must calculate controllable ad uncontrollable consumption loads per every percentage of demand response for every demand response between 0% to 45%. To this end, the following hypotheses are considered: If the demand response is 0%, a controllable load is not used. In this case, the number of subscribers is 266. The average consumption load per subscriber and total microgrid load per hour is mentioned in Table 2.

If demand response is 15%, only the first three controllable appliances (washing machine, dishwasher, and dry-cleaner) are used. According to the fact that we have 226 subscribers, the total controllable load is 519 kWh. The uncontrollable load's diagram must be multiplied by a coefficient to calculate consumption loads of 4000 kWh. The reason is that the total consumption load must be the same in every case to compare the results of various cases. It must be valid for 30% and 40% demand response percentages. In the case that demand response is 30%, almost 60% of subscribers use electric cars in addition to the first three appliances (washing machine, dishwasher, and dry-cleaner). In this case, the number of subscribers is 215 to have equal consumption load in different cases. If demand response is 45%, all subscribers use all controllable appliances. Considering 190 subscribers for this case, the total uncontrollable load is as follows (Table 3)

Information about electricity prices bought from the main grid is mentioned in Figure 10. For hours between 7 and 23, the purchase is 0.32 S/kWh while determines 0.12 S/kWh for other hours. The sale price for the main grid is 80% of the purchase price.

Tables (4) and (5) represent economic and technical information and other parameters considered for optimization. Data required by photovoltaic units are mentioned in [37]. To this end, data from [42] is used.

According to the above, the mentioned framework includes some of the recent research through which the framework is explained. Simulation is done for 400 various percentages (0%, 15%, 30%, and 45%) of demand responses to examine the methodology.

TABLE 6. The summarizes the results of the base case.

Summation of battery, power reduction in inverter, power sale to main grid (kWh)	Share of Power purchase from main grid (kWh)	Share of battery (discharging) (kWh)	Share of photovoltaic units (kWh)	Share of wind turbine (kWh)	Value of the load		The effect of demand response on expenses (%)	value of the objective function (J_0) ($)	Load response %
					Controllable (kWh)	Uncontrollable (kWh)			
2109.1	1938.22	1290.65	1673.99	1206.23	0	4000	0	237349	0%
1890.75	1843.88	1088.85	1520.2	1437.82	518.7	3481.3	-%4.2	227389	15%
1585.94	1577.47	898.55	1401.9	1708.02	1193.3	2806.7	-%7.06	220590	30%
1248.77	1389.46	640.79	1336.8	1881.72	1510.5	2489.5	-%9.14	215653	45%

TABLE 7. Appliances installed in the residential microgrids for the base case.

Inverter capacity (kW)	Battery capacity (kWh)	Photovoltaic capacity (kW)	The capacity of wind turbine (kW)	Demand response
199	1784	283	375	0%
182	1413	257	477	15%
169	1151	237	531	30%
124	972	226	585	45%

A. BASE CASE (BC)

The current case study assumes that the uncertainty parameters related to wind power, solar energy, and demand equal the predicted values. The base case must be calculated for the objective function in the first stage. To this end, the uncertainty of wind and photovoltaic generation is not taken into account to focus on the determination of optimized annual expenses, equipment optimized sizes required for grid design, and explaining the role of productive resources in meeting demands. Total expenses of microgrid design are mentioned by (41), which is the summation of the purchase price, operation and maintenance expenses, and replacement and exchange prices. The related data is mentioned in Table 6. The objective function value for every percentage of demand response is sent to the second optimization level to conduct case study B. Additionally, the total consumption of energy and cooperation degree of generators in meeting demands (including purchasing power from the main grid, wind unit, photovoltaic unit, and battery which charge itself by discharging) is mentioned in the same Table for every percentage of demand response. In the last column of the same Table, battery charging capacity and the power sold to the main grid are mentioned. Figure 11 depicts the convergence of the objective function in the simulation of case study B for a demand response of 0% done based on ACO. According to this figure, the ACO managed to find the converged optimized response after 221 repetitions. Additionally, it is evident that the objective function starts at 245622 USD and goes to 237349 USD at the end.

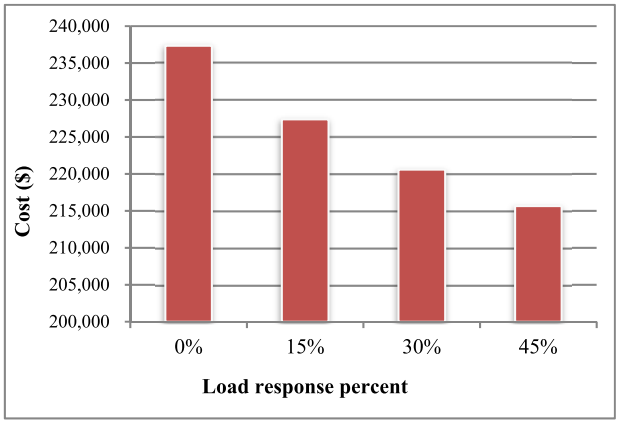

FIGURE 12. The effect of demand response on the objective function.

Despite complications of the optimization problem, ACO managed to find the optimized response to reduce the objective function into the converged value. The time interval for solving the optimization problem is taken 500 repetitions based on ACO. Consequently, we consider 50 particles, and the time would be 2 minutes. Table 7 represents appliances installed in the microgrid used in the current case study simulation. According to this Table, an increasein demand response leads to a reduction in battery capacity. The main battery in the microgrid can increase operational capacity by transporting consumption loads. Therefore, there is less need for batteries in times of increased demand responses because of the increase in the ability of consumption loads transportation. The increase in demand response leads to a reduction in the capacity of photovoltaic units, which may boost the capacity of wind units. An increase in demand response may cause higher delivery of consumption loads, leading to frequent usage of wind units and fewer photovoltaic ones.

The objective function for various demand response percentages is shown in Figure 12. So that, Increasing the amount of this percentage may reduce the microgrid's expenses. If demand response is not considered, the total microgrid expense is 237349 USD. Consideration of a 15% demand response leads to a 4.2% reduction in expenses. In this case,

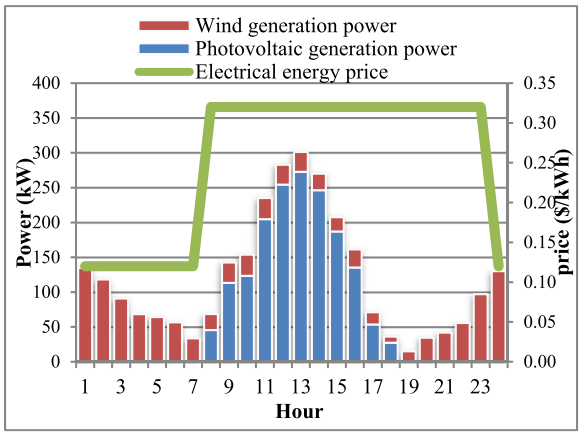

(a)

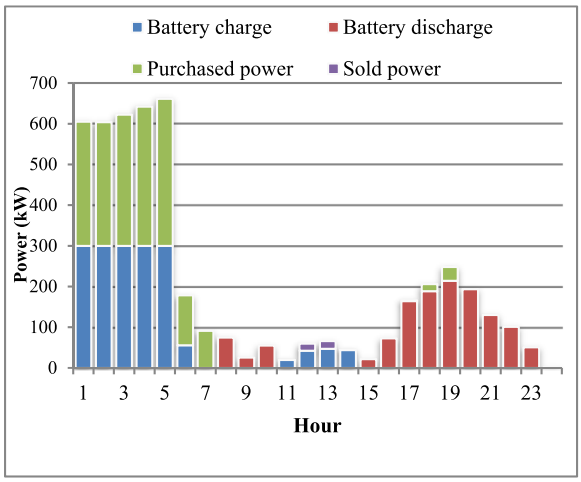

(b)

FIGURE 13. Power distribution over microgrid for the base case (a), and demand response of 0% (b).

the grid expense is 227389 USD. 30% and 45% increase in demand response can reduce expenses by 7.06% and 9.14%.

In the following, the distribution of operational power and consumption loads in a residential microgrid for 24 hours is simulated and evaluated concerning various percentages of demand response in the base case (A). Simulation of other cases leads to the same results; thus, the power distribution of case A is evaluated. Figure 13 shows power distribution over the microgrid while demand response is not considered. According to this figure, the wind unit operational capacity increases in the early and late hours of the day, while photovoltaic units increase at midday. As for charge and discharge ability, electricity is cheaper between 1:00 and 7:00 when microgrid demand is lower. Excess power is purchased from the main grid to charge the battery.

On the other hand, electricity is expensive between 8:00 and 23:00 when the battery is used to meet microgrid demand to reduce costs. Obviously, between 11:00 and 14:00, when the photovoltaic generation is high, a part of that power is used to charge the battery. Then, the battery can be used in the early hours of the night when the photovoltaic unit generates

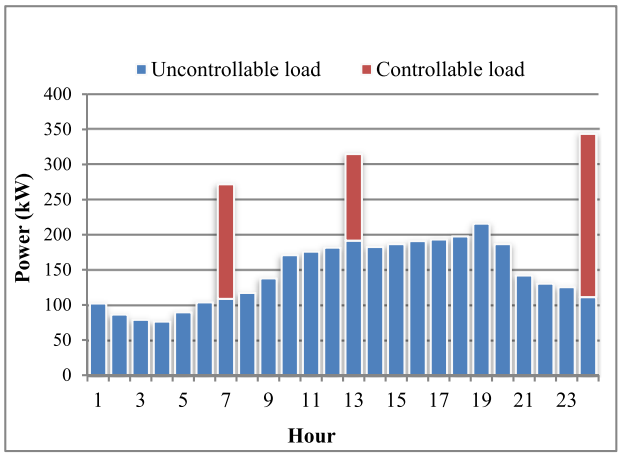

(a)

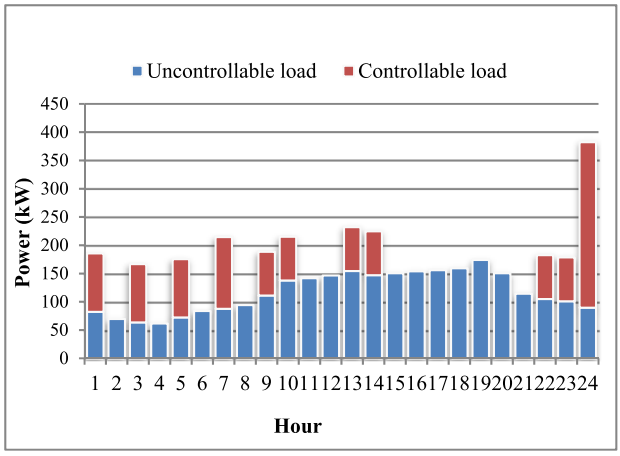

(b)

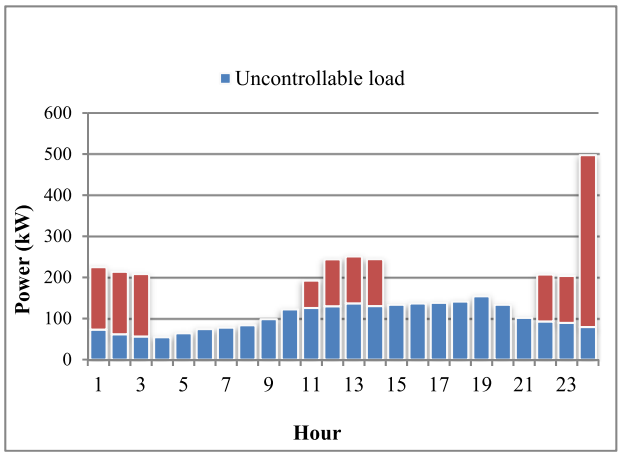

(c)

FIGURE 14. Consumption load of the microgrid for load response 15% (a), load response 30% (b), and load response 45% (c).

no power. Additionally, the wind unit meets the demand at 24:00 when the photovoltaic unit has no generation. Since renewable units have the highest generation at 12:00 - 13:00, some of that power is sold to the grid at midday. Power distribution over the microgrid can be optimized to reduce expenses.

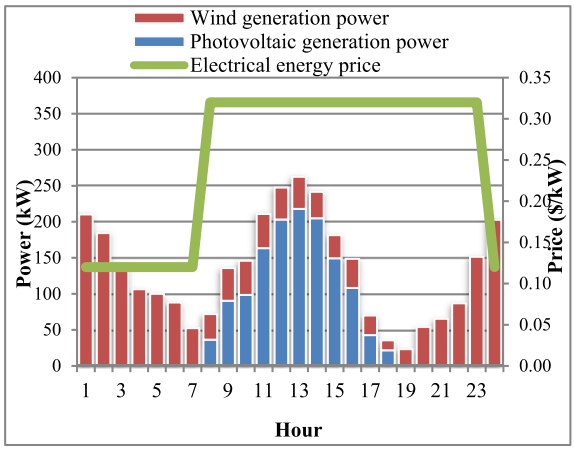

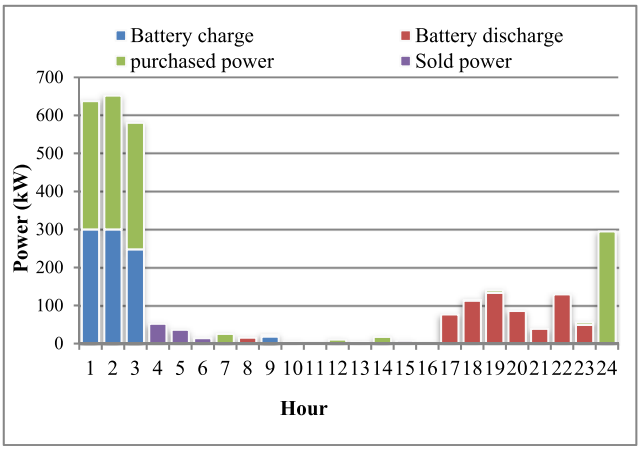

FIGURE 15. The power distribution of the microgrid for state 1 of the simulation for demand response of 45%.

The distribution of controllable loads for various demand responses is shown in Figure 14. As for demand response of 15%, controllable loads are postponed to 7:00 and 24:00 when electricity is cheap. A part of the controllable load is delivered to 13:00 when photovoltaic generation is high and the grid is loaded with the excess load. As for demand response of 30%, a part of controllable is delivered to 1:00, 3:00, 5:00, 7:00, and 24:00 when electricity is cheap. A part of the consumption load goes to low-demand hours (between 9:00 and 14:00 when photovoltaic generation is high or between 22:00 and 23:00 when the grid is asked for lower demand). As for demand response of 45%, a part of the consumption load is delivered to 1:00, 2:00, 3:00, and 24:00 when electricity is cheap. Another part is time-restricted and cannot be delivered in cheap hours. In this case, desired times can be 11:00 and 14:00 when photovoltaic generation is high or 22:00 and 23:00 when the grid faces less demand. Therefore, distribution is done in a way that grid expenses may reduce.

Power distribution over microgrid for demand response of 45% is shown in Figure 15. It is shown that wind generation is considered in the early and late hours of the day, while photovoltaic generation is the best option at midday. Between 1:00

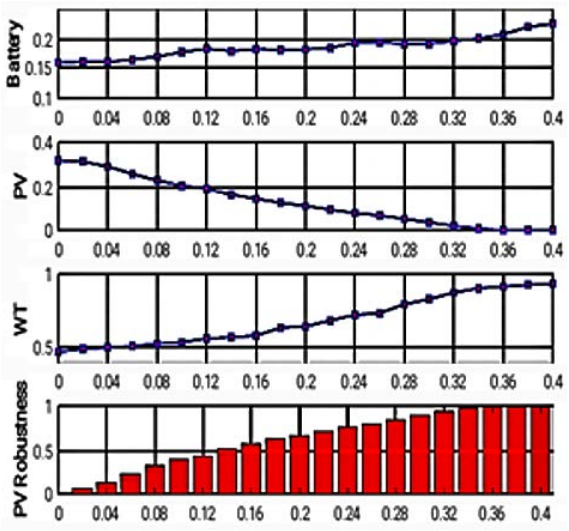

FIGURE 16. Changes made by different parameter choices in B-1.

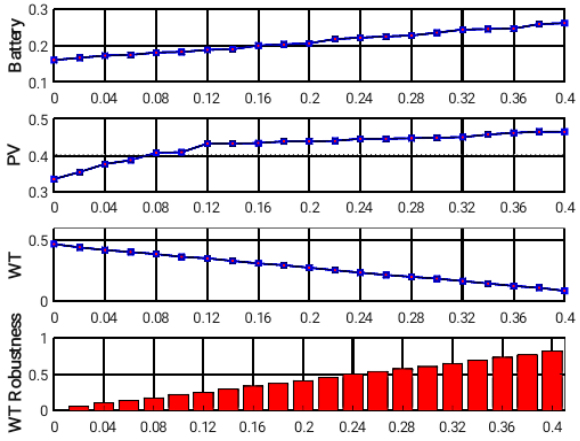

FIGURE 17. Changes while using different parameters in B-2.

and 7:00, when electricity is cheap and the demand is low, the line's share of the power is bought from the main grid to charge the battery and meet controllable loads. Between 8:00 and 16:00, photovoltaic units can meet consumer demand. Therefore, there is no need to purchase the power or discharge the battery. Between 17:00 and 23:00, when photovoltaic generation reduces and controllable demands must be met, batteries are discharged into the grid. Obviously, at 24:00, when electricity is cheap and photovoltaic generation is zero, the main part of power is purchased from the main grid to meet consumption demands. Distribution over the microgrid represents the optimized power distribution at various hours to reduce microgrid expenses.

B. RISK-AVERSE STRATEGY (RAS)

In a case study (A) which is called the base case, uncertainty parameters related to solar energy, wind power, and demand are equal to the predicted ones. Optimization based on optimized power distribution is evaluated regardless of

TABLE 8. Summary of results obtained from B-1 for demand response of 45%.

control ς_cValue %	Cost function ($)	Value of the load		Wind unit		Photovoltaic unit			battery	
		Controllable (kWh)	uncontrollable (kWh)	Capacity value (kWh)	Share (kWh)	Capacity value (kWh)	Share (kWh)	The maximum radius of uncertainty	Capacity value (kWh)	Share of discharge (kWh)
0	215653	1510	2489	585	1881.72	226	1336.8	0	972	640.79
2	219966	1510	2489	607	1952.5	226	1253.95	0.062	977	644.76
4	224280	1510	2489	620	1994.3	226	1163.04	0.130	977	646.23
6	228592	1510	2489	632	2032.9	226	1030.70	0.229	994	660.18
8	232905	1510	2489	654	2103.7	226	906.37	0.322	996	681.75
10	237218	1510	2489	665	2139.1	226	811.45	0.393	1018	711.84
12	241531	1510	2489	698	2245.2	226	752.63	0.437	1056	734.33
14	245844	1510	2489	708	2277.4	226	652.37	0.512	1063	719.26
16	250157	1510	2489	722	2322.4	226	572.16	0.572	1122	731.58
18	254471	1510	2489	790	2541.1	226	499.97	0.626	1128	728.73
20	258784	1510	2489	800	2573.3	226	442.49	0.669	1128	729.88
22	263097	1510	2489	851	2737.3	226	374.31	0.720	1133	742.18
24	267410	1510	2489	899	2891.7	226	311.48	0.767	1169	773.94
26	271723	1510	2489	914	2940.0	226	267.36	0.800	1172	779.10
28	276036	1510	2489	990	3184.5	226	207.20	0.845	1177	765.56
30	280349	1510	2489	1032	3319.6	226	137.69	0.897	1177	768.79
32	284662	1510	2489	1090	3506.1	226	77.53	0.942	1184	785.95
34	288975	1510	2489	1126	3621.9	226	28.07	0.979	1198	804.16
36	293288	1510	2489	1140	3666.9	226	0	1	1261	831.28
38	297601	1510	2489	1156	3718.4	226	0	1	1306	881.47
40	301914	1510	2489	1166	3750.6	226	0	1	1369	902.94

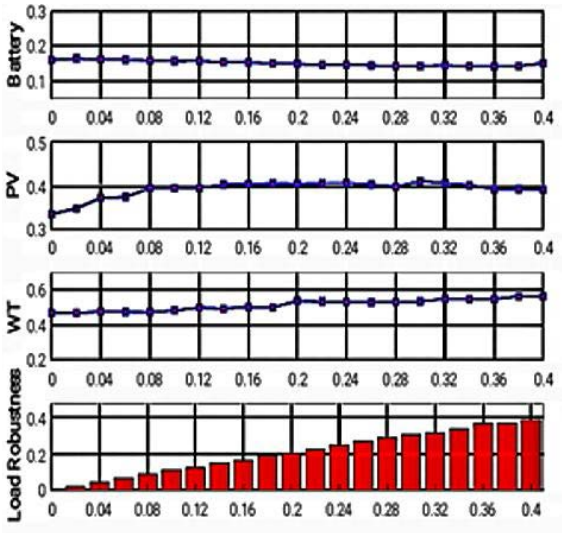

FIGURE 18. Changes caused by various parameters for B-2.

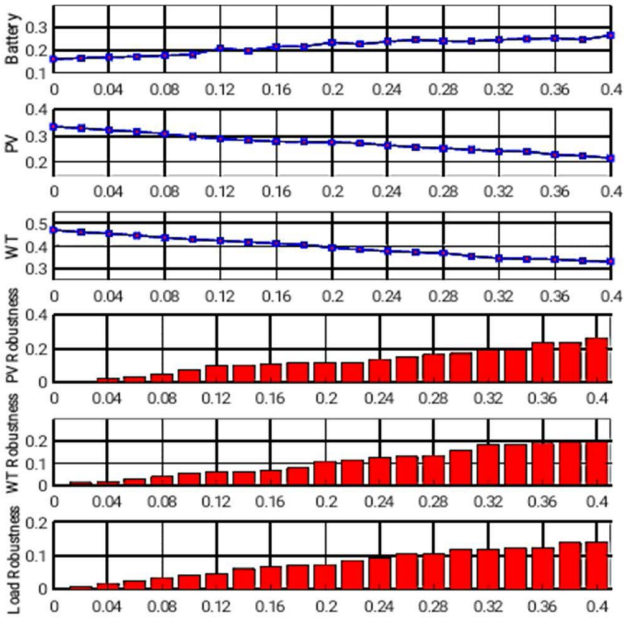

FIGURE 19. Changes forced by various selections of the conservative parameter in B-4.

demand response. In the case of study B, the focus is on determining the maximum uncertainty radius in risk-averse considering excess expenses as a critical point of the objective function. In this case, the designed microgrid's resistance is investigated concerning uncertainty. Additionally, a descriptive investigation of optimized sizes is conducted. This case study focuses on a demand response of 45%.

1) IMPERFECT PV PREDICTION

In this case, it is assumed that distributed power flow during 24 hours is predicted. On the other hand, $\xi^{pd} = 0$. Accordingly, demand and supply are the same. Also, it is assumed that wind speed is predicted and $\xi^{wt} = 0$. In a photovoltaic system, a reduction in predicted power can negatively affect the objective function. In other words, expenses rise. According to (46), photovoltaic generation reduces to calculate the maximum uncertainty radius. In this case, ς_c goes from 0 to 40%. It aims to determine the microgrid's

TABLE 9. Results of B-2 with the demand response of 45%.

Control value ς_c %	Cost function ($)	Value of the load		Wind unit			Photovoltaic unit		Battery	
		Controllable (kWh)	Uncontrollable (kWh)	Capacity value (kWh)	Share (kWh)	The maximum radius of uncertainty	Capacity value (kWh)	Share (kWh)	Capacity value (kWh)	Share (Discharge) (kWh)
0	215653	1510	2489	585	1881.72	0	226	1336.8	972	640.79
2	219966	1510	2489	585	1772.58	0.058	239	1413.7	1011	666.05
4	224280	1510	2489	585	1682.26	0.106	254	1502.5	1048	689.39
6	228592	1510	2489	585	1618.28	0.140	261	1543.9	1060	697.28
8	232905	1510	2489	585	1550.53	0.176	275	1626.7	1103	724.22
10	237218	1510	2489	585	1460.21	0.224	276	1632.6	1109	729.61
12	241531	1510	2489	585	1409.41	0.251	292	1727.2	1147	752.72
14	245844	1510	2489	585	1324.73	0.296	292	1727.2	1156	760.08
16	250157	1510	2489	585	1241.93	0.340	293	1733.2	1203	801.16
18	254471	1510	2489	585	1181.72	0.372	296	1750.9	1219	813.38
20	258784	1510	2489	585	1100.80	0.415	296	1750.9	1231	824.58
22	263097	1510	2489	585	1016.13	0.460	297	1756.8	1300	872.05
24	267410	1510	2489	585	937.09	0.502	301	1780.5	1323	886.93
26	271723	1510	2489	585	861.82	0.542	301	1780.5	1339	900.78
28	276036	1510	2489	585	797.85	0.576	302	1786.4	1351	910.92
30	280349	1510	2489	585	739.51	0.607	303	1792.3	1390	1092.11
32	284662	1510	2489	585	656.72	0.651	304	1798.2	1444	976.49
34	288975	1510	2489	585	575.80	0.694	309	1827.8	1457	982.68
36	293288	1510	2489	585	498.65	0.735	312	1845.5	1463	987.21
38	297601	1510	2489	585	436.55	0.768	314	1857.4	1539	1037.29
40	301914	1510	2489	585	334.94	0.822	314	1857.4	1545	1046.75

resistance in a risk-averse method. Considering $J_0 + |J_0|\,\varsigma_c$ The maximum uncertainty radius of the photovoltaic unit in the risk-averse method is determined. Table 8 summarizes the results of the case study. It is shown that the power supplied by the photovoltaic system is kept fixed while ς_c increases as expected. This Table mentions the power supplied by the various resources, objective function, and total energy consumption. It is worth noting that the energy supplied by the battery is calculated based on discharged power. Figure 16 shows the changes in different options against ς_c. As it is shown, an increase in ς_c may lead to a reduction in photovoltaic generation and its role in supplying demands. Accordingly, bigger batteries and wind units are designed for the microgrid to increase the generation of wind units and batteries. According to the figure, when $\varsigma_c = 36\%$ and expenses soar by 36%, uncertainty is 1 for the photovoltaic unit. On the other hand, the microgrid cannot meet demands when the uncertainty for the photovoltaic unit is 1.

2) IMPERFECT WT PREDICTION

The effect of uncertainty on wind turbines is investigated. In a risk-averse strategy, wind turbines behave similarly to photovoltaic units. A reduction in the predicted power can negatively affect the objective function. This way, expenses increase. According to (45), wind turbine generation reduces risk-averse strategy. It is assumed that the power flow is

TABLE 10. Summary of results of B-3 for demand response of 45%.

Control value ς_c %	Cost function ($)	Value of the load			Wind turbine		Photovoltaic unit		Battery	
		Controllable (kWh)	Uncontrollable (kWh)	The maximum radius of uncertainty	Capacity value (kWh)	Share (kWh)	Capacity value (kWh)	Share (kWh)	capacity value (kWh)	Share (discharge) (kWh)
0	215653	1510	2489	0	585	1881.72	226	1336.8	972	640.79
2	219966	1544.73	2546.24	0.023	595	1913.88	240	1419.6	1023	672.92
4	224280	1580.97	2605.98	0.047	620	1994.30	263	1555.7	1033	676.49
6	228592	1614.19	2660.74	0.069	630	2026.47	270	1597.1	1049	686.99
8	232905	1644.39	2710.52	0.089	641	2061.85	290	1715.4	1062	693.43
10	237218	1677.61	2765.27	0.111	667	2145.48	296	1750.9	1067	696.03
12	241531	1698.75	2800.12	0.125	697	2241.98	300	1774.6	1086	707.07
14	245844	1738.01	2864.83	0.151	707	2274.15	313	1851.5	1089	708.63
16	250157	1762.17	2904.66	0.167	730	2348.13	319	1886.9	1099	714.15
18	254471	1793.88	2956.93	0.188	741	2383.51	325	1922.4	1100	714.98
20	258784	1822.57	3004.22	0.207	806	2592.59	330	1952	1101	717.54
22	263097	1854.28	3056.49	0.228	816	2624.76	336	1987.5	1105	715.42
24	267410	1889.01	3113.73	0.251	826	2656.92	343	2028.9	1131	736.61
26	271723	1919.21	3163.51	0.271	837	2692.31	346	2046.7	1132	733.63
28	276036	1949.41	3213.29	0.291	857	2756.64	347	2052.6	1132	733.93
30	280349	1973.57	3253.12	0.307	868	2792.02	362	2141.3	1155	747.23
32	284662	1993.20	3285.48	0.320	903	2904.60	362	2141.3	1171	764.14
34	288975	2021.89	3332.77	0.339	914	2939.99	363	2147.2	1175	759.87
36	293288	2067.19	3407.44	0.369	934	3004.32	363	2147.2	1181	772.63
38	297601	2074.74	3419.88	0.3740	964	3100.82	364	2153.1	1206	785.66
40	301914	2098.90	3459.71	0.390	976	3139.42	367	2170.9	1231	836.80

predicted for 24 hours and $\xi^{\mathrm{pd}} = 0$. Consequently, predicted demand and actual demand are the same. Additionally, the output of the photovoltaic system exceeds the predicted value and $\xi^{\mathrm{pv}} = 0$. Under these circumstances, ς_c changes from 0 to 40% to determine the maximum uncertainty radius to increase wind turbine output. It aims to determine microgrid resistance in risk-averse strategy when expenses for designing microgrid change from 0 to 40%. Table 9 is a summary of the results of this case study. In this Table, power supplied by different resources is mentioned. Figure 17 represents the role of various options against ς_c. Accordingly, an increase in ς_c may lead to a decrease in wind turbine output. Therefore, bigger photovoltaic units and batteries are required to increase power generation. The bigger batteries and PV cells lead to increased expenses in this case. According to figure 3, $\varsigma_c = \%40$ and $\xi^{\mathrm{wt}} = 82.2\%$, only 17.8% of the predicted wind power meets demands.

3) IMPERFECT LOAD PREDICTION

Compared to the previous cases, the effect of load uncertainty is investigated here. Therefore, it is assumed that solar energy and wind speed are predicted, and PV output and wind power are the same as the predicted values. It means that $\xi^{pv} = \xi^{wt} = 0$. In wind turbines and PV units, a decrease in the predicted value can negatively affect objective function, increasing expenses. According to (47), system load is increased to

TABLE 11. Summarized the results of B-4 with a demand response of 45%.

Control value ς_c %	Cost function ($)	Value of the load			Wind unit			Photovoltaic unit			battery	
		Controllable (kWh)	Uncontrollable (kWh)	The maximum radius of uncertainty	Capacity value (kWh)	Share (kWh)	The maximum radius of uncertainty	Capacity value (kWh)	Share (kWh)	The maximum radius of uncertainty	Capacity value (kWh)	Share (discharge) (kWh)
0	215653	1510	2489	0	585	1881.72	0	226	1336.8	0	972	640.79
2	219966	1523.59	2512.41	0.009	585	1859.14	0.012	226	1326.14	0.008	1006	664.13
4	224280	1537.18	2534.82	0.018	585	1849.73	0.017	226	1304.75	0.024	1032	682.33
6	228592	1549.26	2554.74	0.026	585	1829.03	0.028	226	1291.38	0.034	1062	703.05
8	232905	1562.85	2577.15	0.035	585	1808.33	0.039	226	1271.33	0.049	1097	727.23
10	237218	1571.91	2592.09	0.041	585	1780.11	0.054	226	1235.23	0.076	1131	751.06
12	241531	1580.97	2607.03	0.047	585	1768.81	0.060	226	1205.82	0.098	1162	873.04
14	245844	1602.11	2641.89	0.061	585	1766.93	0.061	226	1199.14	0.103	1195	837.44
16	250157	1612.68	2659.32	0.068	585	1753.76	0.068	226	1188.44	0.111	1223	921.88
18	254471	1617.21	2666.79	0.071	585	1734.94	0.078	226	1183.10	0.115	1238	924.58
20	258784	1620.23	2671.77	0.073	585	1676.61	0.109	226	1180.42	0.117	1343	1003.66
22	263097	1639.86	2704.14	0.086	585	1665.32	0.115	226	1179.09	0.118	1343	982.17
24	267410	1650.43	2721.57	0.093	585	1642.74	0.127	226	1153.69	0.137	1429	1038.46
26	271723	1667.04	2748.96	0.104	585	1637.09	0.130	226	1134.97	0.151	1484	1086.70
28	276036	1668.55	2751.45	0.105	585	1627.69	0.135	226	1116.25	0.165	1546	1063.58
30	280349	1688.18	2783.82	0.118	585	1584.41	0.158	226	1105.56	0.173	1568	1068.66
32	284662	1689.69	2786.31	0.119	585	1537.36	0.183	226	1080.16	0.192	1604	1099.18
34	288975	1692.71	2791.29	0.121	585	1531.72	0.186	226	1078.82	0.193	1617	1120.94
36	293288	1697.24	2798.76	0.124	585	1524.19	0.190	226	1022.68	0.235	1645	1136.76
38	297601	1718.38	2833.62	0.138	585	1516.66	0.194	226	1018.67	0.238	1655	1121.01
40	301914	1722.91	2841.09	0.141	585	1507.26	0.199	226	981.23	0.266	1781	1211.04

calculate the maximum uncertainty radius in the RA strategy. Table 10 is a summary of the results obtained from this case study. It is shown that power supplied by PV unit is kept fixed while ς_c; increases as expected. Figure 18 shows the changes caused by different energy resources. Figure 6 is a comparison between every resource and its base value when ς_c; changes from 0 to 24%. It is evident that the energy fed by ESS increases while ς_c goes up while it has the same effect for both $\varsigma_c = 0$ and $\varsigma_c = 20\%$.

4) IMPERFECT WT AND PV LOAD PREDICTION

In cases, B-1, B-2, and B-3, the uncertainty of photovoltaic generation, wind power, and load are investigated, respectively. If the effect of uncertainty on both load and photovoltaic units matches the prediction, a multipurpose maximization problem is solved to determine ξ^{pv} and ξ^{pd}. In the following relation, the weighted sum can be used to solve the optimization problem [43]. This method uses prioritization to select weighted coefficients [44, 45]. To this end, daily photovoltaic generation (primary value) is divided by daily consumption. Therefore, ω_{pd} is taken as the unit value because deviation from the predicted value can significantly affect expenses which are shown in Figures 3 and 5. Table 11 is a summary of results. It is obvious that any changes in ς_c can lead to reduction in photovoltaic generation while load increases. Figure 19 represents the effect of various resources as well as the maximization of uncertainty on photovoltaic generation, wind power and load compared to the conservative parameter of ς_c.

VI. CONCLUSION

In this paper, the first step of microgrid design focuses on demand response based on ant colony optimization (ACO). Results have shown that using demand response in all scenarios reduces expenses because there is no longer a need to install batteries and generation units while controllable loads are transferred to cheap hours. Additionally, it is indicated

that Power distribution, charge, and discharge reduce microgrid expenses. Then, an IGDT-based framework is proposed for microgrid design. Also, the uncertainty of photovoltaic generation, wind power, and load is determined for the microgrid to calculate the expenses of photovoltaic, wind, and load generation while deviation is examined based on IGDT. Results have shown that considering excess expenses in the base case is the easiest way to determine the maximum uncertainty radius for photovoltaic generation, wind power, and load to keep the grid stable. According to the IGDT, the results are valid. Additionally, this method is more expensive while designers and owners of the microgrid believe in its efficiency.

CONFLICT OF INTEREST

The authors declare that they have no known competing financial interests or personal relationships that could have appeared to influence the work reported in this paper.

DATA SHARING AND DATA AVAILABILITY

The datasets used and analyzed during the current study are available from the corresponding author on reasonable request.

REFERENCES

[1] Z. Wang, B. Chen, J. Wang, J. Kim, and M. M. Begovic, "Robust optimization based optimal DG placement in microgrids," *IEEE Trans. Smart Grid*, vol. 5, no. 5, pp. 2173–2182, Sep. 2014.

[2] S. Mizani and A. Yazdani, "Design and operation of a remote microgrid," in *Proc. 35th Annu. Conf. IEEE Ind. Electron.*, Nov. 2009, pp. 4299–4304.

[3] J. P. Fossati, A. Galarza, A. Martín-Villate, and L. Fontán, "A method for optimal sizing energy storage systems for microgrids," *Renew. Energy*, vol. 77, pp. 539–549, May 2015.

[4] J. Burrows, E. Scheier, C. Smith, J. Smith, A. Young, and T. Young, "Comparative life cycle assessment of a Thai Island's diesel/PV/wind hybrid microgrid," *Renewable Energy*, vol. 80, pp. 85–100, Aug. 2015.

[5] N. Amiri, M. Shaterabadi, K. Reza Kashyzadeh, and M. Chizari, "A comprehensive review on design, monitoring, and failure in fixed offshore platforms," *J. Mar. Sci. Eng.*, vol. 9, no. 12, p. 1349, Nov. 2021.

[6] L. Wen, K. Zhou, S. Yang, and X. Lu, "Optimal load dispatch of community microgrid with deep learning based solar power and load forecasting," *Energy*, vol. 171, pp. 1053–1065, Mar. 2019.

[7] W. Y. Chiu, H. Sun, and H. V. Poor, "A multiobjective approach to multimicrogrid system design," *IEEE Trans. Smart Grid*, vol. 6, no. 5, pp. 2263–2272, Sep. 2015.

[8] H. Farzin, R. Ghorani, M. Fotuhi-Firuzabad, and M. Moeini-Aghtaie, "A market mechanism to quantify emergency energy transactions value in a multi-microgrid system," *IEEE Trans. Sustain. Energy*, vol. 10, no. 1, pp. 426–437, Jan. 2019.

[9] L. Wang, B. Zhang, Q. Li, W. Song, and G. Li, "Robust distributed optimization for energy dispatch of multi-stakeholder multiple microgrids under uncertainty," *Appl. Energy*, vol. 255, Dec. 2019, Art. no. 113845.

[10] J. M. Rey, P. P. Vergara, J. Solano, and G. Ordóñez, "Design and optimal sizing of microgrids," in *Microgrids Design Implementation*. Cham, Switzerland: Springer, 2019, pp. 337–367.

[11] A. Zidan, H. A. Gabbar, and A. Eldessouky, "Optimal planning of combined heat and power systems within microgrids," *Energy*, vol. 93, pp. 235–244, Dec. 2015.

[12] P. Moutis, S. Skarvelis-Kazakos, and M. Brucoli, "Decision tree aided planning and energy balancing of planned community microgrids," *Appl. Energy*, vol. 161, pp. 197–205, Jan. 2016.

[13] S. Li, H. He, Y. Chen, M. Huang, and C. Hu, "Optimization between the PV and the retired EV battery for the residential microgrid application," *Energy Proc.*, vol. 75, pp. 1138–1146, Aug. 2015.

[14] T. M. Priya, V. Sanjana, B. Gohila, R. Lavanya, A. Anbazhagan, M. Veerasundaram, and L. Ramesh, "Design and analysis of a sustainable LV residential microgrid," *Proc. Technol.*, vol. 21, pp. 139–146, Jan. 2015.

[15] A. Arabali, M. Ghofrani, M. Etezadi-Amoli, and M. S. Fadali, "Stochastic performance assessment and sizing for a hybrid power system of solar/wind/energy storage," *IEEE Trans. Sustain. Energy*, vol. 5, no. 2, pp. 363–371, Apr. 2014.

[16] C. K. Ekman, "On the synergy between large electric vehicle fleet and high wind penetration—An analysis of the Danish case," *Renew. Energy*, vol. 36, no. 2, pp. 546–553, Feb. 2011.

[17] L. Göransson, S. Karlsson, and F. Johnsson, "Integration of plug-in hybrid electric vehicles in a regional wind-thermal power system," *Energy Policy*, vol. 38, no. 10, pp. 5482–5492, Oct. 2010.

[18] S. Kahrobaee, S. Asgarpoor, and W. Qiao, "Optimum sizing of distributed generation and storage capacity in smart households," *IEEE Trans. Smart Grid*, vol. 4, no. 4, pp. 1791–1801, Dec. 2013.

[19] Q. Zhang, T. Tezuka, K. N. Ishihara, and B. C. Mclellan, "Integration of PV power into future low-carbon smart electricity systems with EV and HP in kansai area, Japan," *Renew. Energy*, vol. 44, pp. 99–108, Aug. 2012.

[20] A. Botterud, Z. Zhou, J. Wang, J. Sumaili, H. Keko, J. Mendes, R. J. Bessa, and V. Miranda, "Demand dispatch and probabilistic wind power forecasting in unit commitment and economic dispatch: A case study of Illinois," *IEEE Trans. Sustain. Energy*, vol. 4, no. 1, pp. 250–261, Jan. 2013.

[21] Y. Guo, M. Pan, Y. Fang, and P. P. Khargonekar, "Decentralized coordination of energy utilization for residential households in the smart grid," *IEEE Trans. Smart Grid*, vol. 4, no. 3, pp. 1341–1350, Sep. 2013.

[22] N. Kunwar, K. Yash, and R. Kumar, "Area-load based pricing in DSM through ANN and heuristic scheduling," *IEEE Trans. Smart Grid*, vol. 4, no. 3, pp. 1275–1281, Sep. 2013.

[23] E. Matallanas, M. Castillo-Cagigal, A. Gutiérrez, F. Monasterio-Huelin, E. Caamaño-Martín, D. Masa, and J. Jiménez-Leube, "Neural network controller for active demand-side management with PV energy in the residential sector," *Appl. Energy*, vol. 91, no. 1, pp. 90–97, Mar. 2012.

[24] A.-H. Mohsenian-Rad and A. Leon-Garcia, "Optimal residential load control with price prediction in real-time electricity pricing environments," *IEEE Trans. Smart Grid*, vol. 1, no. 2, pp. 120–133, Sep. 2010.

[25] A.-H. Mohsenian-Rad, V. W. S. Wong, J. Jatskevich, R. Schober, and A. Leon-Garcia, "Autonomous demand-side management based on game-theoretic energy consumption scheduling for the future smart grid," *IEEE Trans. Smart Grid*, vol. 1, no. 3, pp. 320–331, Dec. 2010.

[26] A. Molderink, V. Bakker, M. G. C. Bosman, J. L. Hurink, and G. J. M. Smit, "Management and control of domestic smart grid technology," *IEEE Trans. Smart Grid*, vol. 1, no. 2, pp. 109–119, Sep. 2010.

[27] M. Vasirani, R. Kota, R. L. G. Cavalcante, S. Ossowski, and N. R. Jennings, "An agent-based approach to virtual power plants of wind power generators and electric vehicles," *IEEE Trans. Smart Grid*, vol. 4, no. 3, pp. 1314–1322, Sep. 2013.

[28] M. A. Jirdehi and M. Shaterabadi, "A low-carbon strategy using INVELOX turbines in the presence of real-time energy price uncertainty," *Greenhouse Gases, Sci. Technol.*, vol. 11, pp. 461–482, Mar. 2021.

[29] M. Shaterabadi and M. A. Jirdehi, "Smart scheduling of transmission line switching: Optimization of multi-objective microgrid's day-ahead energy scheduling with considering high penetration of green energies and INVELOX," *Electr. Eng.*, vol. 103, pp. 1753–1767, Jan. 2021.

[30] M. Shaterabadi and M. A. Jirdehi, "Multi-objective stochastic programming energy management for integrated INVELOX turbines in microgrids: A new type of turbines," *Renew. Energy*, vol. 145, pp. 2754–2769, Jan. 2020.

[31] S. V. Raygani, R. Sharma, and T. K. Saha, "PV power output uncertainty in Australia," in *Proc. IEEE Power Energy Soc. Gen. Meeting*, Jul. 2015, pp. 1–5.

[32] A. Soroudi, "Possibilistic-scenario model for DG impact assessment on distribution networks in an uncertain environment," *IEEE Trans. Power Syst.*, vol. 27, no. 3, pp. 1283–1293, Aug. 2012.

[33] A. Soroudi and A. Rabiee, "Optimal multi-area generation schedule considering renewable resources mix: A real-time approach," *IET Gener., Transmiss. Distrib.*, vol. 7, no. 9, pp. 1011–1026, Sep. 2013.

[34] M. Urbina and Z. Li, "A fuzzy optimization approach to PV/battery scheduling with uncertainty in PV generation," in *Proc. 38th North Amer. Power Symp.*, Sep. 2006, pp. 561–566.

[35] P. Chen, P. Siano, Z. Chen, and B. Bak-Jensen, "Optimal allocation of power-electronic interfaced wind turbines using a genetic algorithm-monte Carlo hybrid optimization method," in *Wind Power Systems*. Cham, Switzerland: Springer, 2010, pp. 1–23.

[36] A. Soroudi and T. Amraee, "Decision making under uncertainty in energy systems: State of the art," *Renew. Sustain. Energy Rev.*, vol. 28, pp. 376–384, Dec. 2013.
[37] R. Atia and N. Yamada, "Sizing and analysis of renewable energy and battery systems in residential microgrids," *IEEE Trans. Smart Grid*, vol. 7, no. 3, pp. 1204–1213, May 2016.
[38] D. Ke, F. Shen, C. Y. Chung, C. Zhang, J. Xu, and Y. Sun, "Application of information gap decision theory to the design of robust wide-area power system stabilizers considering uncertainties of wind power," *IEEE Trans. Sustain. Energy*, vol. 9, no. 2, pp. 805–817, Apr. 2018.
[39] M. Charwand and Z. Moshavash, "Midterm decision-making framework for an electricity retailer based on information gap decision theory," *Int. J. Electr. Power Energy Syst.*, vol. 63, pp. 185–195, Dec. 2014.
[40] K. Zare, M. P. Moghaddam, and M. K. Sheikh-El-Eslami, "Risk-based electricity procurement for large consumers," *IEEE Trans. Power Syst.*, vol. 26, no. 4, pp. 1826–1835, Nov. 2011.
[41] S. Nojavan, K. Zare, and M. R. Feyzi, "Optimal bidding strategy of generation station in power market using information gap decision theory (IGDT)," *Electr. Power Syst. Res.*, vol. 96, pp. 56–63, Mar. 2013.
[42] S. Feng and C. L. P. Chen, "A fuzzy restricted Boltzmann machine: Novel learning algorithms based on the crisp possibilistic mean value of fuzzy numbers," *IEEE Trans. Fuzzy Syst.*, vol. 26, no. 1, pp. 117–130, Feb. 2018.
[43] A. Rabiee, S. Nikkhah, A. Soroudi, and E. Hooshmand, "Information gap decision theory for voltage stability constrained OPF considering the uncertainty of multiple wind farms," *IET Renew. Power Gener.*, vol. 11, no. 5, pp. 585–592, Apr. 2017.
[44] N. Rezaei, A. Ahmadi, A. H. Khazali, and J. M. Guerrero, "Energy and frequency hierarchical management system using information gap decision theory for islanded microgrids," *IEEE Trans. Ind. Electron.*, vol. 65, no. 10, pp. 7921–7932, Oct. 2018.
[45] A. Soroudi, A. Rabiee, and A. Keane, "Information gap decision theory approach to deal with wind power uncertainty in unit commitment," *Electric Power Syst. Res.*, vol. 145, pp. 137–148, Apr. 2017.

MEHRDAD MOVAHEDPOUR is currently pursuing the Ph.D. degree in electrical engineering with Islamic Azad University, Yasouj Branch. He is also a member of the Faculty of Yasuj Technical and Vocational University and the Head of the Engineering System Organization of KB Province. His specialized scientific and research fields are power systems, microgrids, power network control, photovoltaic, and intelligence controller.

MOHAMMAD JAVAD KIANI was born in Yasouj, Iran. He received the B.S. and M.S. degrees in electrical engineering from the K. N. Toosi University of Technology, Tehran, Iran, in 2003 and 2008, respectively, and the Ph.D. degree in electrical engineering from Universiti Teknologi Malaysia (UTM), Johor, Skudai, Malaysia, in 2017. He is currently a Faculty Member with the Department of Electrical Engineering, Islamic Azad University, Yasouj. His current research interests include nanotechnology and application, power electronics, power systems, controllers, and intelligence networks.

MAHMOUD ZADEHBAGHERI was born in Yasouj, Iran, in October 1979. He received the B.S. degree in electrical engineering from Kashan University, in 2003, the M.S. degree in electrical engineering from Islamic Azad University, Najafabad Branch, in 2008, and the joint Ph.D. degree in electrical engineering from Universiti Teknologi Malaysia (UTM), Johor, Skudai, Malaysia, and Hakim Sabzvari University, in 2017. He is with the Department of the Electrical Engineering, Islamic Azad University, Yasouj. His research interests include the fields of power electronics, electrical machines and drives, FACTS devices, renewable energy, and power quality.

SIRUS MOHAMMADI was born in Mamasani, Fars, Iran, in September 1974. He received the B.S. degree in electrical engineering from Chamran University, Ahvaz, in 2000, the M.S. degree in electrical engineering from Shiraz University, in 2005, and the Ph.D. degree in electrical engineering from Science and Research Branch, Islamic Azad University, in 2014. He is with the Faculty Member of the Electrical Engineering Department, Islamic Azad University of Gachsaran. His research interests include the fields of power systems, reliability of power systems, FACTS devices, and distribution networks.